Geophysical Research Letters

RESEARCH LETTER
10.1029/2020GL091461

Key Points:

- Negative trends of chlorophyll anomaly dominate in cold-core rings (CCRs) while both positive and negative trends exist in warm-core rings (WCRs)
- Short-term fluctuations of chlorophyll anomaly are closely correlated with mixed layer depth and sea surface temperature anomaly
- CCRs can be distinctly less productive than WCRs in the same seasons

Supporting Information:

- Supporting Information S1

Correspondence to:
K. Chen,
kchen@whoi.edu

Citation:
Ning, J., Chen, K., & Gaube, P. (2021). Diverse variability of surface chlorophyll during the evolution of Gulf Stream rings. *Geophysical Research Letters*, *48*, e2020GL091461. https://doi.org/10.1029/2020GL091461

Received 27 OCT 2020
Accepted 9 FEB 2021

Diverse Variability of Surface Chlorophyll During the Evolution of Gulf Stream Rings

Jue Ning[1,2], Ke Chen[2], and Peter Gaube[3]

[1]College of Oceanography, Hohai University, Nanjing, Jiangsu, China, [2]Physical Oceanography Department, Woods Hole Oceanographic Institution, Woods Hole, MA, USA, [3]Applied Physics Laboratory, University of Washington, Seattle, WA, USA

Abstract We investigate how the near-surface chlorophyll (CHL)-a evolves in Gulf Stream (GS) warm-core rings (WCRs) and cold-core rings (CCRs) using multi-platform satellite observations. Averaged CHL anomaly (CHLA) within the rings exhibits both positive and negative linear trends during the evolution of the WCRs while negative trends dominate in CCRs. This difference is associated with a variety of physical processes occurring during the evolution process. Meanwhile, eddy-centric analysis reveals four spatial patterns of CHLA long-term trends, some of which highlights the importance of rings in shaping surface CHL. Short-term fluctuations of CHLA in WCRs and CCRs are closely correlated with mixed layer depth and sea surface temperature anomaly and highlight the complex interplay between multiple mechanisms. In addition, we find higher concentration CHL in some WCRs than that in CCRs during the same season, providing an alternative view of the characteristics of the surface ecosystem in Gulf Stream rings.

Plain Language Summary The highly energetic and large-amplitude mesoscale eddies of the Gulf Stream (GS) region, often referred to as GS rings, have significant influence on biogeochemical environment and marine ecosystem through various mechanisms. Although the importance of GS rings has been recognized, contrasting results exist regarding the role of the GS rings in the upper-ocean ecosystem. For a better understanding of mesoscale physical and biological interactions, here we examine the temporal and spatial variability of near-surface chlorophyll (CHL), and how it is modulated by the physical processes during individual ring's life span from satellite observations in details. Remarkable long-term and short-term variabilities, and different spatial patterns are found in both warm-core rings (WCRs) and cold-core rings (CCRs). Strikingly, the result shows that WCRs are more productive than CCRs during the decay stage, which is in contrast to the existing understanding. This study provides a comprehensive observational perspective of surface CHL variations associated with mesoscale eddies from formation to decay.

1. Introduction

Mesoscale eddies with spatial scales of O (100 km), play a fundamental role in physical-biological-biogeochemical interactions in the upper ocean (e.g., McGillicuddy, 2016). The largest amplitude eddies are often found in western boundary current systems, such as the Gulf Stream (GS). Long-lived and large-amplitude GS eddies, often referred to as GS rings, are generated when meanders of the GS pinch off. In general, they are classified into two types: anticyclonic warm-core rings (WCRs) and cyclonic cold-core rings (CCRs). WCRs are usually found between the GS and the continental slope, trapping relatively warm and low chlorophyll (CHL) Sargasso Sea water during formation (e.g., Gangopadhyay et al., 2020; Joyce, 1985; Ryan et al., 2001); CCRs are most often located to south of the GS, trapping cold and higher CHL slope water from the north of the GS (Pingree et al., 1979; The Ring Group, 1981; Figures 1a and 1b).

The importance of the rings in transporting and redistributing heat, nutrients, and phytoplankton, has been long recognized (e.g., Chen et al., 2014, 2020; Franks et al., 1986; Gaube et al., 2014, 2019; McGillicuddy & Robinson, 1997; Olson, 1986). Traditional ship-based surveys provide detailed sampling of a targeted ring, but this approach usually needs to balance the spatial resolution and synopticity, and only a limited number of rings can be sampled (e.g., Fox & Kester, 1986; McCarthy & Nevins, 1986; McGillicuddy et al., 1998, 2007). Alternatively, satellite measurements of ocean color and sea surface height provide a synoptic view

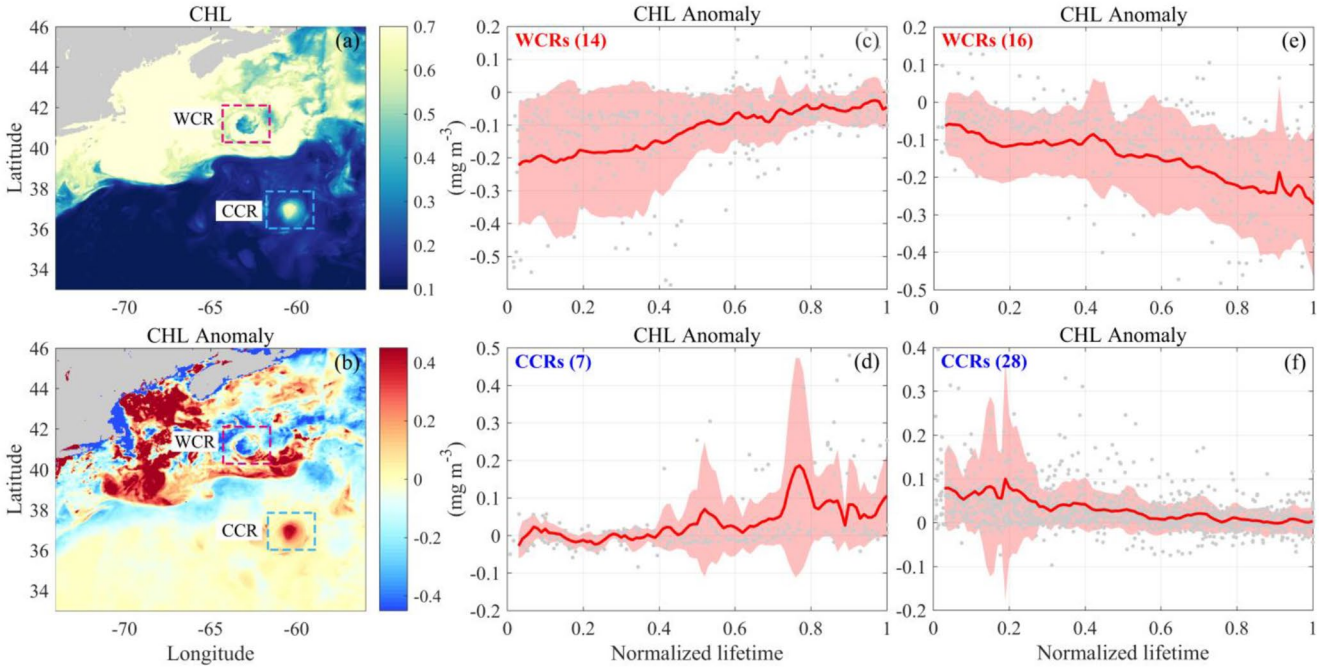

Figure 1. CHL (a), CHLA (b) in a typical WCR and CCR on May 5, 2012, and time series of the composite CHLA (c)–(f) in 14 WCRs and 7 CCRs with positive linear trends ($p < 0.1$), (c)–(d), 16 WCRs and 28 CCRs with negative linear trends ($p < 0.1$), (e)–(f), respectively. Data based on level-4 data along with gray dots in (c)–(f) indicate values of level-3 data (see Section 2.2 for the description of the data). Shaded area represents one standard deviation. CCR, cold-core ring; CCRs, cold-core rings; CHL, chlorophyll; CHLA, chlorophyll anomaly; WCR, warm-core ring; WCRs, warm-core rings.

of the physical-biological interactions in GS rings at a fine spatiotemporal resolution (García-Moliner & Yoder, 1994; Gaube et al., 2014; Gaube & McGillicuddy, 2017; Siegel et al., 2011). Based on multi-year satellite data, previous studies have suggested that cyclonic eddies are associated with enriched phytoplankton biomass and anticyclonic eddies are generally characterized by depressed biomass in the GS region (e.g., Gaube et al., 2014; Siegel et al., 2011). In the meantime, other studies based on field observations have revealed high biomass/productivity in some anticyclonic eddies (e.g., Nelson et al., 1985, 1989; Smith & Baker, 1985; Yentsch & Phinney, 1985). The contrasting variability of ecosystem characteristics associated with eddies in the GS region complicate the understandings of mesoscale physical-biological interactions in the upper ocean. Furthermore, during the evolution of rings, which can last from days to months, surface ecosystem and chlorophyll in an eddy can be modulated by a number of physical and biological processes. As a result, the ecosystem characteristics can be highly variable at any given time during the evolution of rings. For a better understanding of mesoscale physical and biological interactions, it is necessary to examine the temporal and spatial variability of surface CHL, and how it is modulated by the physical processes during a ring's life span.

In this study, we investigate CHL evolution over the entire lifecycle of WCRs and CCRs using 15-year multi-platform satellite observations in the GS region of the Northwest Atlantic (30°–50°N, 50°–80°W). We attempt to capture the characteristics of surface CHL during the evolution of GS rings, further examine the similarities and differences of CHL response in WCRs and CCRs, and understand the underlying mechanisms. This study provides a comprehensive observational perspective of surface CHL variations associated with mesoscale eddies from formation to decay, and thus help us gain a deeper understanding of the role of mesoscale eddies in regulating the upper ocean ecosystem.

2. Data and Methods

2.1. Mesoscale Eddy Atlas and Gulf Stream Rings Detection

A mesoscale eddy atlas based on altimeter-derived sea level anomaly (SLA) was used (Schlax & Chelton, 2016). This dataset provides polarity information, location, time series, amplitude, eddy radius, and rotational speed of each identified eddy. More details of this methodology are provided by Chelton et al. (2011).

One important step in this work is to identify the GS rings from the general mesoscale eddies, which could be very different in biophysical characteristics: GS rings generally have larger vertical scale, amplitude and radius, and can only be found in the open ocean off the continental shelf. Therefore, we apply a series of selection criteria to the mesoscale eddy dataset. The criteria are: the maximum amplitude, radius and lifetime of rings must be no less than 25 cm, 50 km, and 21 days, respectively; they have to shed off the GS; the locations of WCRs must be between the GS, which is defined as the 25 cm Sea Surface Height contour (Andres, 2016), and the shelf break, defined here as the 200 m isobath. Ultimately, 46 WCRs and 61 CCRs are identified from 2003 to 2017 (Table S1). One issue we notice is that at times the eddy center from the original eddy atlas is not consistent with the local SLA extremum, which could make the eddy-centric analysis (see below) biased. Accordingly, additional steps are taken by combining the real time SLA data and the eddy dataset to re-locate the position of the identified ring. We added two more criteria: first, the eddy center is always located at a local SLA extremum and only SLA peaks within the diameter of the ring are considered. So, if the center of an eddy does not reside at a local SLA extremum, we shift the center to the nearest local SLA extremum within the radius. Second, the distance between two consecutive eddy centers has to be smaller than 86.4 km, which is equivalent to the distance in one day advected with 1 m s^{-1} speed in the slope sea. This restriction excludes some of the sudden shifts of eddy locations in the original dataset. In addition, some manual adjustments are made to track the same SLA peak as much as possible. For example, during the merging of two eddies, the eddy center would jump back and forth between the two eddies. The manual adjustment would then designate the eddy center to the more robust eddy to reduce the "jumps" of eddy locations. We also exclude the days when the SLA extrema no longer exist within the rings toward the end of the rings' lifecycles. Throughout, the interior of a ring is defined as the area within half of the radius (R).

2.2. Multi-Platform Chlorophyll Dataset

The daily surface CHL during 2003–2017 with spatial resolution of 4 km from the Copernicus-GlobColour project is used in this study. This is a merged product based on multiple satellite sensors (SeaWiFS, MODIS, MERIS, VIIRS-SNPP&JPSS1, and OLCI-S3A&S3B) to maximize the data coverage. The cloud-free level-4 data used here is based on optimal interpolation that uses kriging method and regional anisotropic covariance models provided by Copernicus-Marine Environment Service (Saulquin et al., 2019). CHL anomaly (CHLA) is further calculated by subtracting daily CHL values from the corresponding daily climatology from the dataset. To evaluate the accuracy of the GlobColour level-4 data, we compare the level-3 and level-4 data, and find a high degree of consistency (e.g., Figure 4b). The results discussed below are mainly based on level-4 data, but we note that using level-3 data can well reproduce the same results (e.g., Figures S4 and S5), despite some minor differences due to the missing values in level-3 data. In addition, we also independently reconstructed level-3 MODIS CHL using Data Interpolating Empirical Orthogonal Functions (DINEOF) method (Alvera-Azcárate et al., 2005; Beckers & Rixen, 2003). By performing Empirical Orthogonal Functions iteratively, the DINEOF method seeks to fill missing CHL data due to cloud coverage using the inherent temporal and spatial modes. In comparison, the DINEOF reconstructed MODIS CHL and GlobColour level-4 products are largely consistent (not shown), in both spatial pattern and temporal variability. For this study, we only show the results based on GlobColour CHL.

2.3. Oceanic and Atmospheric Factors

The National Oceanic and Atmospheric Administration (NOAA) daily Advanced Very High Resolution Radiometer-Only Optimally Interpolated Sea Surface Temperature (OISST) data on a global 1/4° grid are used (Reynolds et al., 2007). In order to obtain a comparable time series of sea surface temperature anomaly (SSTA) with CHL anomaly in GS rings, a daily mean climatology for the period 2003–2017 is calculated and subsequently removed from the daily OISST.

Mixed layer depth (MLD) data from GLobal Ocean ReanalYsis and Simulation (GLORYS) are used to help examine the vertical physical process. This is a data-assimilated product and is available daily with a 1/12° horizontal resolution. Comparisons (not shown) with altimeter observations show that GLORYS captures the surface characteristics of the rings very well.

Gridded surface vector winds on a global 1/4° grid from the Cross-Calibrated Multi-Platform and surface net heat flux (HF) with a spatial resolution of 25 km from ECMWF ERA5 reanalysis (Hersbach et al., 2020) are also used. The daily mean climatology for the period 2003–2017 is calculated and subsequently removed from the daily HF to obtain HF anomaly (HFA).

3. Results

3.1. Overall Trends of CHL Anomaly, Amplitude and SSTA

The trajectories, spatiotemporal information and characteristics of the selected 46 WCRs and 61 CCRs are summarized in Figure S1, Tables S1, and S2. The mean radius of WCRs and CCRs is 66.0 and 66.9 km, and the mean lifetime is 60 and 70 days, respectively. The minimum and maximum amplitudes in WCRs and CCRs are similar. The maximum lifespan, radius, and rotational speed in CCRs can reach 159 days, 163 km, and 161.5 cm s^{-1}, respectively, which are significantly greater than those in WCRs. Generally, CCRs have longer lifetime, larger radius, amplitude, and rotational speed than WCRs.

To understand the lowest-order variability, we produce composite mean CHLA during the evolution of the GS Rings. Although the averaged CHLA in all 46 WCRs shows complex variability (Figure S2), the CHLA in 14 WCRs has significant positive trend (Figure 1c). In contrast, the CHLA in 16 WCRs (Figure 1e) has significant negative trend, revealing the diverse biophysical characteristics in these WCRs. The amplitude of WCRs tends to increase and decrease in the first 20% and last 60% of WCRs' lifecycles, respectively, suggesting that these WCRs intensify and stabilize briefly and then gradually decay. Besides, there is a good correspondence between increasing CHLA and decreasing SSTA (Figures S3a and S3c). This negative correlation implies the potential control of temperature field on the surface CHL distribution, and is consistent with previous studies (e.g., R. He et al., 2010; McGillicuddy et al., 2001), which examine the concurrent correlation between mesoscale SST and ocean color over different time scales.

For CCRs, the composite mean CHLA has a continuous tendency to decline, with many small fluctuations (Figure S2). Note that those individual CCRs without a significant trend partly impact the overall trend of the composite mean CHLA. As the case for WCRs, there are also two opposite trends in CCRs (Figures 1d and 1f). Rather surprisingly, the dominant trend of CHLA in CCRs is negative. This result highlights the different processes associated with the evolution of WCRs and CCRs, which could be related to the lack of effective mechanisms in delivering deep nutrients to the upper water column in CCRs. For example, vertical mixing is generally stronger in WCRs due to the weaker stratification in comparison to CCRs, which favors nutrients enrichment in the euphotic layer. In addition, eddy-induced Ekman pumping is always positive (upwelling) in WCRs and negative (downwelling) in CCRs. This might account for the smaller number of positive CHLA trends in CCRs. These CCRs have complete lifecycles, as can be seen from Figures S3h and S3k, including the intensification, mature and decay stages. In general, there is no simple linear relationship between SSTA and CHLA in CCRs due to the nonmonotonic variations of SSTA.

3.2. Spatial Patterns of CHL Anomaly Trend

To better understand the similarities and differences regarding the long-term evolution and distribution of surface CHL inside and outside GS rings, we explore the spatial structures of linear trends of CHLA. Multiple spatial patterns of the linear trend of CHLA are identified, which can be categorized into two major types: a negative-dominant (ND) type (Figures 2a–2d) and a positive-dominant (PD) type (Figures 2e–2h), based on the long-term CHLA variability in the center of the rings. The result implies that CHL in rings could either decrease or increase during the life spans. Additionally, the amounts of ND (14) and PD (10) types in WCRs are close to each other, however, in CCRs the ND (24) type is markedly more than the PD (7) type. This is consistent with the results in Section 3.1 and highlights the different processes occurring in these rings.

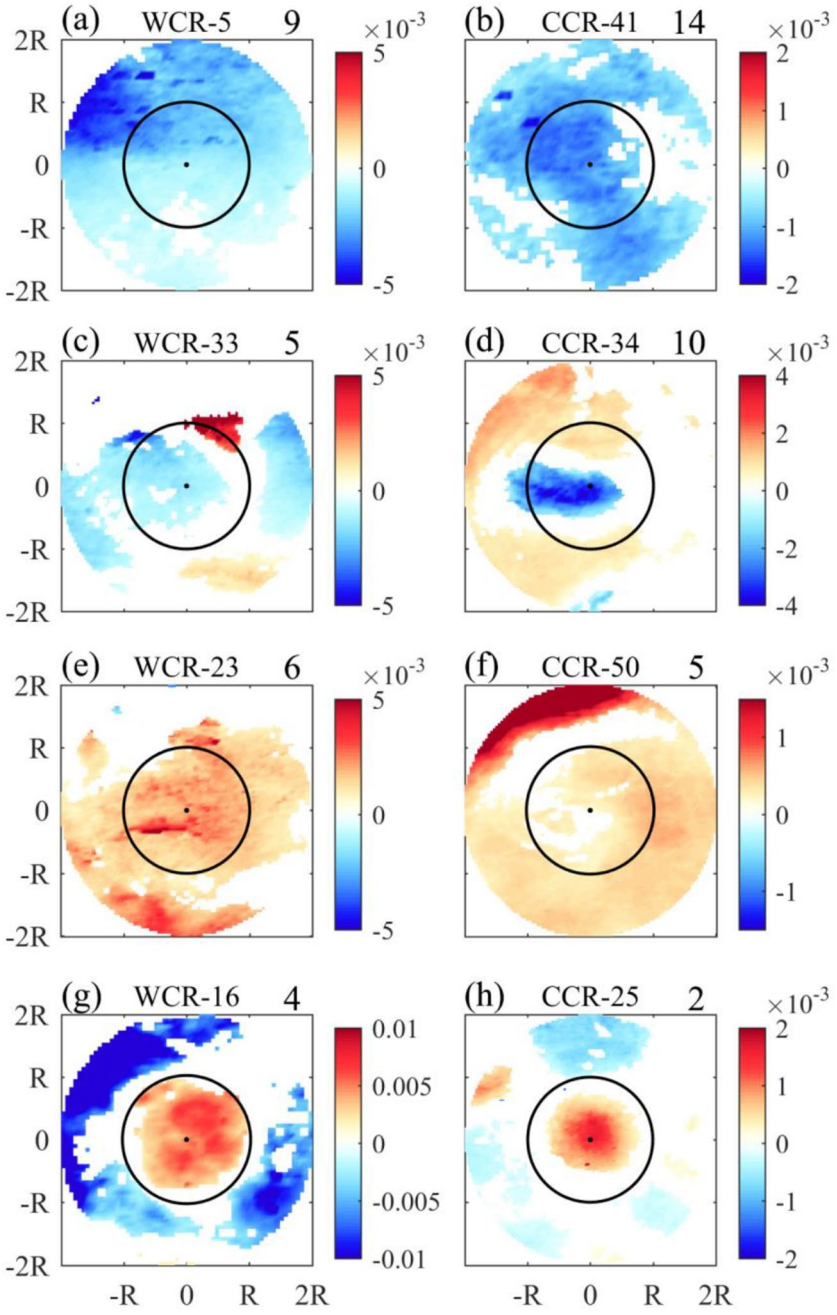

Figure 2. Linear trends distributions of CHLA of WCR-5 (a), 33 (c), 23 (e), 16 (g) and CCR-41 (b), 34 (d), 50 (f) and 25 (h). The solid black circle denotes the maximum eddy radius R. Linear trends with significant level exceeding 90% are plotted. The numbers on top of each panel represent the number of cases. CCR, cold-core ring; CHLA, chlorophyll anomaly; WCR, warm-core ring.

There are two different patterns in both ND and PD types when comparing the variabilities inside and outside of the rings. One is that the linear trends inside and outside the ring have the same sign (Figures 2a, 2b, 2e, and 2f), and the other is that different linear trends exist (Figures 2c, 2d, 2g, and 2h). In particular, as shown in Figures 2d, 2g, and 2h, in some rings, diametrically opposite trends appear inside and outside. More importantly, these special patterns account for a non-negligible portion in both WCRs and CCRs and reflect the importance of mesoscale ocean processes in shaping the surface CHL distributions. On the other

hand, the patterns with the same sign suggest that larger-scale forcing, beyond mesoscale processes, acts as the dominant driver (Figures 2a, 2b, 2e, and 2f).

3.3. Short-Term Fluctuations of CHL Anomaly

Short-term fluctuations in CHLA are partially responsible for the complex temporal evolution of these anomalies. In order to investigate the underlying mechanisms that trigger the short-term variability of CHLA, we further analyze the co-variability of atmospheric and oceanic variables (Figure 3). It turns out that among all variables, the fluctuations of CHLA in WCRs are primarily related to the changes of MLD. Note that both positive and negative correlations between MLD and CHLA exist, suggesting MLD is associated with the variation of CHLA through different processes. For example, the deepening of mixed layer could induce stronger entrainment of subsurface nutrients to the upper ocean (Dufois et al., 2016; Q. He et al., 2019). This is particularly relevant for WCRs because of the weaker stratification. Alternatively, the enhanced mixing with deeper mixed layer could entrain subsurface CHL maximum into the surface layer (Dufois et al., 2017; Xing et al., 2019), and thus increase the CHL concentration. On the other hand, the shallowing of mixed layer could concentrate the total amount of CHL in the mixed layer, resulting in an increase in the surface layer. All these processes can occur within a given ring, potentially explaining the coexisting positive and negative correlations.

For CCRs, the highest correlation is found between SSTA and CHLA. Higher CHLA is often associated with negative SSTA. This result is consistent with earlier findings (e.g., R. He et al., 2010; McGillicuddy et al., 2001), which suggest that the displacement isopycnals from the subsurface would enrich the nutrients content and increase the surface CHL due to the subsurface CHL maximum (Michaels et al., 1994). In reality, either the ventilation of the isotherms or near-surface diapycnal mixing (e.g., as a result of surface wind stress), would need to occur to produce the negative SSTA and deliver nutrients and CHL to the surface. It is also worth noting that in CCRs, significant correlation is found between CHLA and SSTA, but the variabilities of SSTA and MLD are not always consistent. The inconsistency can be understood from the consideration that MLD is modulated by several other processes including surface buoyance and momentum forcing as well as vertical shear so the positive or negative SSTA itself does not necessarily imply a shallower or deeper MLD.

As is shown in Figure 3, the evolution of CHLA in two typical examples (i.e., WCR-27 and CCR-32) presents remarkable short-term variations throughout their entire lifecycles. In WCR-27, the short-term variation of CHLA is positively associated with MLD ($r = 0.39$, linearly detrended, $p < 0.1$). Specifically, Period A1 (B1; marked with "A1" ["B1"] in Figure 3a) with distinct fall (rise) of CHLA corresponds to relatively weaker (stronger) wind and shallower (deeper) MLD, and positive (negative) HFA. As discussed above, the deeper mixed layer in the rings can lead to more nutrients entrained into the euphotic zone, based on which CHL concentrations increase.

In CCR-32, the short-term variation of SSTA has a negative effect on CHLA ($r = -0.44$, $p < 0.05$). For instance, the decreasing CHL in Period A2 (Figure 3b) is concurrent with a maximum of SSTA, along with relatively shallow MLD, and less strong wind. The maximum CHLA (~0.1 mg m^{-3}) occurs in Period B2, when the mixed layer reaches its deepest depth (~65 m). Different short-term fluctuations may be induced by different processes even in the same ring. Therefore, it is important to be mindful when explaining the short-term variations of CHL in observations.

3.4. Comparing CHL in Individual WCRs and CCRs

In the Northwest Atlantic, WCRs are usually located on the northwest side of GS, and CCRs are usually found to the southeast of the GS. It is well recognized that CHL concentrations in CCRs are higher than those in WCRs at the beginning owing to the different water resources, indicating that CCRs are more productive than WCRs (e.g., Gaube et al., 2014; Gaube & McGillicuddy, 2017; McGillicuddy, 2016; Zhang et al., 2018). When comparing CHL concentrations in individual WCRs and CCRs in the same seasons, however, we find that CHL in some CCRs starts higher than WCRs, but ends lower than or almost equal to that in WCRs. This is in direct contrast to the conventional understanding of biophysical characteristics of the rings.

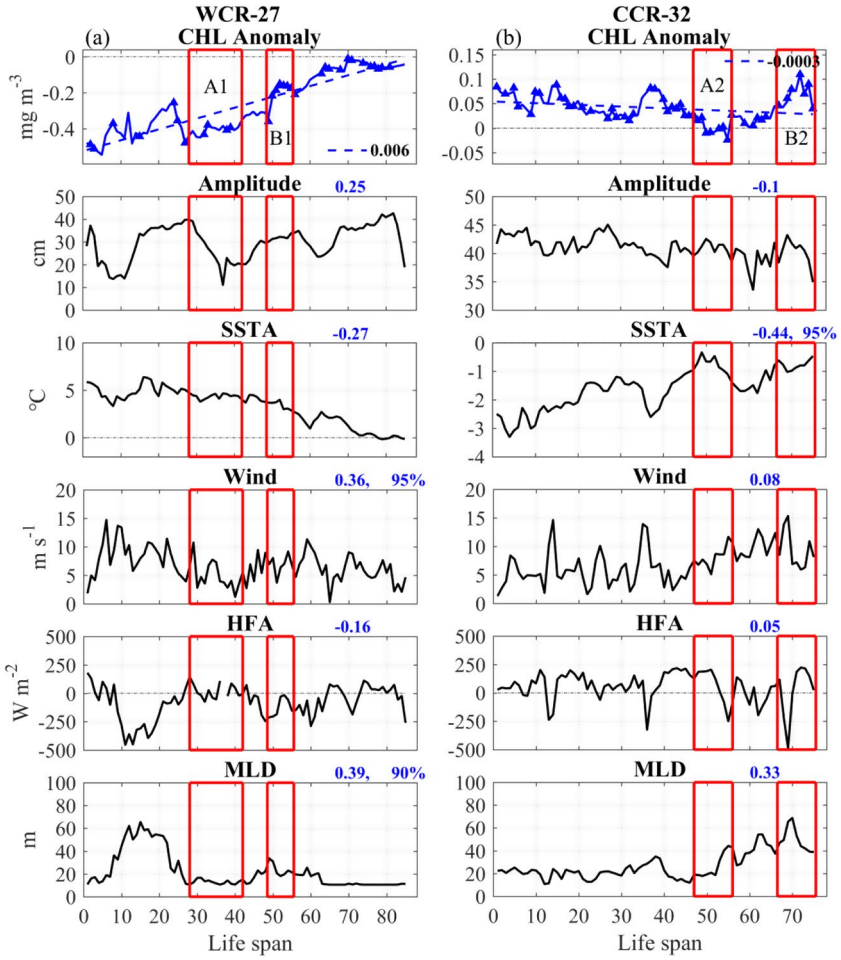

Figure 3. Time series of CHLA, amplitude, SSTA, wind, net heat flux anomaly, and MLD in WCR-27 (a) and CCR-32 (b). The lifespans of WCR-27 and CCR-32 are from April 19, 2012 to July 12, 2012 and from August 17, 2010 to October 30, 2010, respectively. The locations of WCR-27 and CCR-32 where they were first identified are (40.6°N, 61.9°W) and (39.1°N, 56.4°W), respectively. The number on the top of each subpanel represents the correlation coefficient between each variable with CHLA. Significant correlations above 90% level based on t-test are also shown. Blue triangle in the top panel represents the value obtained from level-3 products. Red rectangles highlight two contrasting periods for the WCR and CCR. CCR, cold-core ring; CHLA, chlorophyll anomaly; MLD, mixed layer depth; SSTA, sea surface temperature anomaly; WCR, warm-core ring.

We focus on two groups of rings with similar lifespans (Figure 4). In Group 1, WCRs and CCRs evolve from Spring to Summer and in Group 2 they both evolve from Summer to Fall. Two representative rings WCR-23 and CCR-14 in Group 2 are contrasted. CHL in WCR-23 is about 0.1 mg m^{-3} at the beginning, and ends close to 0.2 mg m^{-3}. In CCR-14, it starts with about 0.2 mg m^{-3} and in the end decreases to 0.1 mg m^{-3}, which is obviously lower than the ending value in WCR-23. Furthermore, the linear trend inside WCR-23 is similar to outside showing a positive trend (Figure 4e). However, although the linear trend outside CCR-14 is also positive, the trend inside CCR-14 is distinctly negative (Figure 4f). This difference results in a significant reduction of CHL concentrations in CCR-14 over the course of its lifespan. Similarly, in Group 1, CHL concentrations inside CCR-34 have a stronger downward trend in the center. Therefore, the lower CHL in CCRs than that in WCRs at the end of lifespan could be attributed to the fact that CCRs are less productive during the decay process. A possible explanation for this result might be that downwelling resulted from eddy pumping, that is, deepening of isopycnals and/or eddy-induced Ekman pumping occurs in decaying CCR-34 and the mixed layer is relatively shallow with the depth not exceeding 15 m (not shown), thereby the nutrients in euphotic zone is not sufficient for sustaining surface phytoplankton. In contrast, mechanisms such as current-induced/vorticity-gradient-induced Ekman pumping and vertical mixing in WCRs could

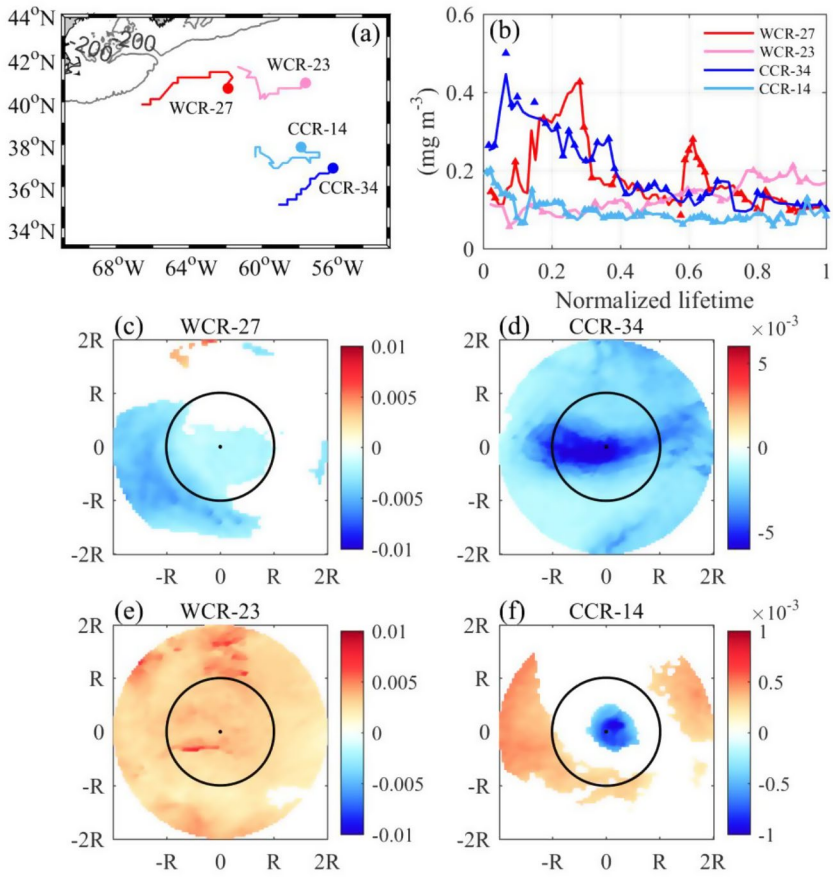

Figure 4. Tracks (a), CHL temporal evolutions (b) and linear trends distributions of CHL of WCR-27 (c), CCR-34 (d), WCR-23 (e), and CCR-14 (f). Red, blue, pink, and cyan colors in (a)–(b) represent Group 1 and Group 2 of rings, respectively. Corresponding colored triangles in (b) represent the value obtained from level-3 products. The solid black circle in (c)–(f) denotes the maximum eddy radius R. Linear trends with significant level exceeding 90% are plotted. CCR, cold-core ring; CHL, chlorophyll; WCR, warm-core ring.

effectively deliver nutrients to the upper ocean and support phytoplankton growth (e.g., Chen et al., 2020). Other factors such as photoadaptation and zooplankton grazing would also impact the variability of surface CHL, but are less straightforward to quantify without sophisticated ecosystem modeling. Nevertheless, our analysis here shows that WCRs have a higher chance of maintaining/increasing the surface CHL concentration than CCRs.

4. Discussion and Summary

Using multi-platform satellite observations, we investigate the evolution of surface CHL in GS rings over their lifecycles. Significant long-term and short-term variabilities of surface CHL exist in both WCRs and CCRs. The numbers of WCRs with long-term positive and negative linear trends are almost equal, but in CCRs the negative trends dominate. These opposite trends probably stem from the combined effects of different physical mechanisms and/or biological-physical interactions. Furthermore, the results highlight the different processes associated with the evolution of WCRs and CCRs, which could be due to the lack of effective physical mechanism in elevating deep nutrients in CCRs. Four diverse spatial patterns observed in the eddy-centric composite average corroborate the discrepancy between two types of rings and reveal that large- and meso-scale dynamics both have effects on surface CHL. Short-term fluctuations of CHLA in WCRs and CCRs are correlated with MLD and SSTA, respectively. The observations of both positive and negative correlations between MLD and CHL anomaly suggest that MLD modulates the variation of CHL anomaly through multiple processes. SSTA is often negatively correlated to CHLA resulting from the

influence of isopycnal displacement and/or near-surface diapycnal mixing on subsurface nutrients and CHL. Finally, considering that long-term downward trends in CCRs account for the majority, it is meaningful to compare CHL concentrations in individual WCRs and CCRs which form and decay in the same seasons. Our results show that initial CHL in some CCRs is higher than in coincident WCRs, but ends lower than, or almost equal, to that in WCRs. This provides an additional view beyond the conventional understanding. The understanding is that downwelling in decaying CCRs, from eddy-induced Ekman pumping and/or eddy pumping, leads to insufficient nutrients in euphotic zone.

We believe that this is the first attempt of detailed investigations of CHL evolution in large anticyclone and cyclone eddies. Results in this study reveal diverse variability of surface CHL in eddies and shed light to the complex roles of mesoscale eddies in upper ocean ecosystem. Constrained by limited observations, it is difficult to distinguish and quantitatively analyze the contribution of different mechanisms to the CHL variability in these GS rings. In that regard, future studies using dedicated observations combined with numerical modeling is warranted to better understand the physical and biological dynamics associated with GS rings.

Data Availability Statement

The eddy identification and tracking dataset is available at AVISO (http://cioss.coas.oregonstate.edu/eddies). The SLA, chlorophyll, and GLORYS12V1 data are available at CMEMS (https://resources.marine.copernicus.eu). The OISST data are available at NOAA ESRL (https://www.esrl.noaa.gov/psd/data/gridded/data.noaa.oisst.v2.highres.html). The surface vector winds are available at RSS (ftp://ftp.remss.com/ccmp). The surface net HF dataset is available at ECMWF (https://www.ecmwf.int/en/forecasts/datasets/reanalysis-datasets/era5).

Acknowledgments
This work was supported by the National Science Foundation Ocean Science Division under grant OCE-1558960. JN was supported by the Fundamental Research Funds for the Central Universities (Hohai University) under grant B200203005 and the China Scholarship Council. The authors thank M. Andres for sharing the Gulf Stream position index.

References

Alvera-Azcárate, A., BarthRixen, A. M., & Beckers, J. M. (2005). Reconstruction of incomplete oceanographic data sets using Empirical Orthogonal Functions: Application to the Adriatic Sea. *Ocean Modelling*, *9*, 325–346. https://doi.org/10.1016/j.ocemod.2004.08.001

Andres, M. (2016). On the recent destabilization of the Gulf Stream path downstream of Cape Hatteras. *Geophysical Research Letters*, *43*, 9836–9842. https://doi.org/10.1002/2016GL069966

Beckers, J. M., & Rixen, M. (2003). EOF calculations and data filling from incomplete oceanographic data sets. *Journal of Atmospheric and Oceanic Technology*, *20*(12), 1839–1856. https://doi.org/10.1175/1520-0426(2003)020<1839:ECADFF>2.0.CO;2

Chelton, D. B., Schlax, M. G., & Samelson, R. M. (2011). Global observations of nonlinear mesoscale eddies. *Progress in Oceanography*, *91*(2), 167–216. https://doi.org/10.1016/j.pocean.2011.01.002

Chen, K., Gaube, P., & Pallàs-Sanz, E. (2020). On the vertical velocity and nutrient delivery in warm core rings. *Journal of Physical Oceanography*, *50*, 1557–1582. https://doi.org/10.1175/JPO-D-19-0239.1

Chen, K., He, R., Powell, B. S., Gawarkiewicz, G. G., Moore, A. M., & Arango, H. G. (2014). Data assimilative modeling investigation of Gulf Stream warm core ring interaction with continental shelf and slope circulation. *Journal of Geophysical Research: Oceans*, *119*, 5968–5991. https://doi.org/10.1002/2014JC009898

Dufois, F., Hardman-Mountford, N. J., Fernandes, M., Wojtasiewicz, B., Shenoy, D., Slawinski, D., et al. (2017). Observational insights into chlorophyll distributions of subtropical South Indian Ocean eddies. *Geophysical Research Letters*, *44*, 3255–3264. https://doi.org/10.1002/2016GL072371

Dufois, F., Hardman-Mountford, N. J., Greenwood, J., Richardson, A. J., Feng, M., & Matear, R. J. (2016). Anticyclonic eddies are more productive than cyclonic eddies in subtropical gyres because of winter mixing. *Science Advances*, *2*(5), e1600282. https://doi.org/10.1126/sciadv.1600282

Fox, M. F., & Kester, D. R. (1986). Nutrient distributions in warm-core ring 82-B April–August. *Deep Sea Research Part I: Oceanographic Research Papers*, *33*, 1761–1772. https://doi.org/10.1016/0198-0149(86)90078-6

Franks, P. J., Wroblewski, J., & Flierl, G. R. (1986). Prediction of phytoplankton growth in response to the frictional decay of a warm-core ring. *Journal of Geophysical Research*, *91*(C6), 7603–7610. https://doi.org/10.1029/JC091iC06p07603

Gangopadhyay, A., Gawarkiewicz, G., Silva, E. N. S., Silver, A. M., Monim, M., & Clark, J. (2020). A census of the warm-core rings of the Gulf Stream: 1980-2017. *Journal of Geophysical Research: Oceans*, *125*(8), e2019JC016033.

García-Moliner, G., & Yoder, J. A. (1994). Variability in pigment concentration in warm-core rings as determined by coastal zone color scanner satellite imagery from the Mid-Atlantic Bight. *Journal of Geophysical Research*, *99*(C7), 14277–14290. https://doi.org/10.1029/93JC03515

Gaube, P., & McGillicuddy, D. J., Jr. (2017). The influence of Gulf Stream eddies and meanders on near-surface chlorophyll. *Deep Sea Research Part I: Oceanographic Research Papers*, *122*, 1–16. https://doi.org/10.1016/j.dsr.2017.02.006

Gaube, P., McGillicuddy, D. J., Jr., Chelton, D. B., Behrenfeld, M. J., & Strutton, P. G. (2014). Regional variations in the influence of mesoscale eddies on near-surface chlorophyll. *Journal of Geophysical Research: Oceans*, *119*, 8195–8220. https://doi.org/10.1002/2014JC010111

Gaube, P., McGillicuddy, D. J., & Moulin, A. J. (2019). Mesoscale eddies modulate mixed layer depth globally. *Geophysical Research Letters*, *46*, 1505–1512. https://doi.org/10.1029/2018gl080006

He, Q., Zhan, H., Xu, J., Cai, S., Zhan, W., Zhou, L., & Zha, G. (2019). Eddy-induced chlorophyll anomalies in the western South China Sea. *Journal of Geophysical Research: Oceans*, *124*, 9487–9506. https://doi.org/10.1029/2019JC015371

He, R., Chen, K., Moore, T., & Li, M. (2010). Mesoscale variations of sea surface temperature and ocean color patterns at the Mid-Atlantic Bight shelfbreak. *Geophysical Research Letters*, *37*, L09607. https://doi.org/10.1029/2010GL042658

Hersbach, H., Bell, B., Berrisford, P., Hirahara, S., Horányi, A., Muñoz-Sabater, J., et al. (2020). The ERA5 global reanalysis. *Quarterly Journal of the Royal Meteorological Society*, *146*, 1999–2049. https://doi.org/10.1002/qj.3803

Joyce, T. M. (1985). Gulf Stream warm-core ring collection: An introduction. *Journal of Geophysical Research*, *90*(C5), 8801–8802. https://doi.org/10.1029/JC090iC05p08801

McCarthy, J. J., & Nevins, J. L. (1986). Sources of nitrogen for primary production in warm-core rings 79-E and 81-D. *Limnology & Oceanography*, *31*, 690–700. https://doi.org/10.4319/lo.1986.31.4.0690

McGillicuddy, D. J. (2016). Mechanisms of physical-biological-biogeochemical interaction at the oceanic mesoscale. *Annual Review of Marine Science*, *8*(1), 125–159. https://doi.org/10.1146/annurev-marine-010814-015606

McGillicuddy, D. J., Anderson, L. A., Bates, N. R., Bibby, T., Buesseler, K. O., Carlson, C. A., et al. (2007). Eddy/wind interactions stimulate extraordinary mid-ocean plankton blooms. *Science*, *316*(5827), 1021–1026. https://doi.org/10.1126/science.1136256

McGillicuddy, D. J., Jr., & Robinson, A. (1997). Eddy-induced nutrient supply and new production in the Sargasso Sea. *Deep Sea Research Part I: Oceanographic Research Papers*, *44*(8), 1427–1450. https://doi.org/10.1016/S0967-0637(97)00024-1

McGillicuddy, D. J., Jr., Robinson, A., Siegel, D., Jannasch, H., Johnson, R., Dickey, T., et al. (1998). Influence of mesoscale eddies on new production in the Sargasso Sea. *Nature*, *394*(6690), 263–266. https://doi.org/10.1038/28367

McGillicuddy, D. J., Kosnyrev, V. K., Ryan, J. P., & Yoder, J. A. (2001). Covariation of mesoscale ocean color and sea-surface temperature patterns in the Sargasso Sea. *Deep Sea Research Part II: Topical Studies in Oceanography*, *48*(8), 1823–1836. https://doi.org/10.1016/S0967-0645(00)00164-8

Michaels, A. F., Knap, A. H., Dow, R. L., Gundersen, K., Johnson, R. J., Sorenson, J., et al. (1994). Seasonal patterns of ocean biogeochemistry at the US JGOFS Bermuda Atlantic time-series study site. *Deep Sea Research Part I: Oceanographic Research Papers*, *41*, 1013–1038. https://doi.org/10.1016/0967-0637(94)90016-7

Nelson, D. M., Ducklow, H. W., Hitchcock, G. L., Brzezinski, M. A., Cowles, T. J., Garside, C., et al. (1985). Distribution and composition of biogenic particulate matter in a Gulf Stream warm-core ring. *Deep Sea Research Part I: Oceanographic Research Papers*, *32*(11), 1347–1369. https://doi.org/10.1016/0198-0149(85)90052-4

Nelson, D. M., McCarthy, J. J., Joyce, T. M., & Ducklow, H. W. (1989). Enhanced near-surface nutrient availability and new production resulting from the frictional decay of a Gulf Stream warm-core ring. *Deep Sea Research Part I: Oceanographic Research Papers*, *36*(5), 705–714. https://doi.org/10.1016/0198-0149(89)90146-5

Olson, D. B. (1986). Lateral exchange within Gulf Stream warm-core ring surface layers. *Deep Sea Research Part I: Oceanographic Research Papers*, *33*(11), 1691–1704. https://doi.org/10.1016/0198-0149(86)90074-9

Pingree, R., Holligan, P., & Mardell, G. (1979). Phytoplankton growth and cyclonic eddies. *Science*, *278*, 245–247. https://doi.org/10.1038/278245a0

Reynolds, R. W., Smith, T. M., Liu, C., Chelton, D. B., Casey, K. S., & Schlax, M. G. (2007). Daily high-resolution-blended analyses for sea surface temperature. *Journal of Climate*, *20*(22), 5473–5496.

Ryan, J., Yoder, J., & Townsend, D. (2001). Influence of a Gulf Stream warm-core ring on water mass and chlorophyll distributions along the southern flank of Georges Bank. *Deep Sea Research Part II: Topical Studies in Oceanography*, *48*(1), 159–178. https://doi.org/10.1016/S0967-0645(00)00117-X

Saulquin, B., Gohin, F., & Fanton d'Andon, O. (2019). Interpolated fields of satellite-derived multi-algorithm chlorophyll-a estimates at global and European scales in the frame of the European Copernicus-Marine Environment Monitoring Service. *Journal of Operational Oceanography*, *12*, 47–57.

Schlax, M. G., & Chelton, D. B. (2016). *The "Growing method" of Eddy identification and tracking in two and three dimensions*. Corvallis, OR: College of Earth, Ocean and Atmospheric Sciences, Oregon State University.

Siegel, D. A., Peterson, P., McGillicuddy, D. J., Maritorena, S., & Nelson, N. B. (2011). Bio-optical footprints created by mesoscale eddies in the Sargasso Sea. *Geophysical Research Letters*, *38*, L13608. https://doi.org/10.1029/2011GL047660

Smith, R. C., & Baker, K. S. (1985). Spatial and temporal patterns in pigment biomass in Gulf Stream warm-core ring 82B and its environs. *Journal of Geophysical Research*, *90*, 8859–8870. https://doi.org/10.1029/JC090iC05p08859

The Ring Group. (1981). Gulf Stream cold-core rings: Their physics, chemistry, and biology. *Science*, *212*, 1091–1100.

Xing, X., Qiu, G., Boss, E., & Wang, H. (2019). Temporal and vertical variations of particulate and dissolved optical properties in the South China Sea. *Journal of Geophysical Research: Oceans*, *124*, 3779–3795. https://doi.org/10.1029/2018JC014880

Yentsch, C. S., & Phinney, D. A. (1985). Rotary motions and convection as a means of regulating primary production in warm core rings. *Journal of Geophysical Research*, *90*, 3237–3284. https://doi.org/10.1029/JC090iC02p03237

Zhang, S., Curchitser, E. N., Kang, D., Stock, C. A., & Dussin, R. (2018). Impacts of mesoscale eddies on the vertical nitrate flux in the Gulf stream region. *Journal of Geophysical Research: Oceans*, *123*, 497–513. https://doi.org/10.1002/2017JC013402.